Post-Translational Modifications Soften Intermediate Filaments

Julia Kraxner,[†] Charlotta Lorenz,[†] Julia Menzel,[‡] Iwan Parfentev,[¶] Ivan Silbern,[¶,§] Henning Urlaub,[¶,§] Blanche Schwappach,[‡,‖] and Sarah Köster[*,†,‖]

[†]*Institute for X-Ray Physics, University of Göttingen, 37077 Göttingen, Germany*

[‡]*Department of Molecular Biology, University Medical Center Göttingen, 37073 Göttingen, Germany*

[¶]*Bioanalytical Mass Spectrometry, Max Planck Institute for Biophysical Chemistry, 37077 Göttingen, Germany*

[§]*Bioanalytic Group, Institute of Clinical Chemistry, University Medical Center Göttingen, 37075 Göttingen, Germany*

[‖]*Cluster of Excellence "Multiscale Bioimaging: from Molecular Machines to Networks of Excitable Cells" (MBExC), University of Göttingen, Germany*

E-mail: sarah.koester@phys.uni-goettingen.de

Abstract

The mechanical properties of biological cells are determined by the cytoskeleton, a composite biopolymer network consisting of microtubules, actin filaments and intermediate filaments (IFs). By differential expression of the cytoskeletal proteins, modulation of the network architecture and the interactions between the filaments, cell mechanics may be adapted to varying requirements on the cell. Here, we focus on the intermediate filament protein vimentin and introduce post-translational modifications as an additional, much faster mechanism for mechanical modulation. We study the impact

of phosphorylation on filament mechanics by recording precise force-strain curves using optical traps. Whereas full phosphorylation leads to disassembly of IFs, partial phosphorylation results in softening of the filaments. We show that binding of the protein 14–3–3 to phosphorylated vimentin IFs further enhances this effect and speculate that in the cell 14–3–3 may serve to preserve the softening and thereby the altered cell mechanics. By employing phosphomimetic mutants and complementary Monte Carlo simulations, we explain our observation through the additional charges introduced during.

The cytoskeleton of eukaryotes consists of three filament systems – microtubules, actin filaments and intermediate filaments (IFs) – which form a complex biopolymer network. The exact composition of the cytoskeleton and the interplay between the three filament types are of great importance as they define the mechanical properties of different cell types.[1] Microtubules and actin filaments are highly conserved throughout cell types and between organisms, whereas more than 70 human genes encode for IFs.[2] Although different IFs are expressed in a cell type specific manner, they all share the same hierarchical assembly pathway from monomers to filaments. The secondary structure of the monomers consists of an α-helical rod domain, flanked by intrinsically disordered head and tail domains.[3,4] During assembly, two monomers align and form parallel coiled-coil dimers, two dimers form antiparallel, half-staggered tetramers, and multiple tetramers constitute a unit-length filament (ULF) (see Fig. 1a). Subsequent longitudinal annealing yields elongated filaments with a diameter of about 10 nm.[5] This hierarchical structure of IFs, in contrast to polar microtubules or actin filaments that elongate by rapid growth at the plus-end, grants IFs their unique mechanical properties.[6–8]

Here, we study the most abundant IF, vimentin, which is found in cells of mesenchymal origin.[5,9] Single vimentin filaments are highly extensible and can be elongated up to at least 4.5 fold.[7,10,11] During elongation, three regimes are observed in the force-strain curves: an initial linear (elastic) increase, a plateau region and a subsequent stiffening.[6,7,12,13] These

different stretching regimes have been linked to structural changes in the rod domain of IFs[12] such as the opening of α helices during the plateau regime.[6,14,15] Additionally, vimentin filaments are able to dissipate large amounts of the input energy while being stretched.[14] Consequently, vimentin IFs act as shock-absorbers for mechanical protection of the cell as well as scaffolds that help to maintain cell shape and organization of the cytoskeleton.[9,16]

An effective way to tune the mechanics of intermediate filaments is the variation of the charges of the amino acids constituting the protein.[17] One cellular mechanism for such charge variation are post-translational modifications (PTMs). Within the IF cytoskeleton, several types of PTMs have been described[18,19] and the most abundantly studied PTM in IFs is phosphorylation, which is involved in regulation of IF dynamics by leading to disassembly and in providing binding sites to signaling proteins.[20,21] It has been shown that the phosphorylation of vimentin by protein-kinase A (PKA) leads to various phosphorylated sites, most of which are positioned in the head region (see Fig. 1a).[21] The importance of the head domain in the assembly process was shown in Refs. 3,22, stressing the obvious link between phosphorylation and assembly dynamics. Although such changes in the molecular interactions during assembly are likely to influence the behavior of the fully assembled filaments, the influence of phosphorylations on filament mechanics is not yet resolved.

A further interesting aspect of phosphorylation is the ability of certain proteins to bind to the modified sites. One such protein is 14–3–3,[23] which is involved in several cellular processes like signal transduction, adhesion and inhibition of tumorigenesis.[24] The role of this protein depends on the interaction partner, *e.g.* it binds to keratin during the cell cycle[25] and affects the assembly dynamics of neurofilaments.[26] However, the role of 14–3–3 for vimentin is unknown.

Here we investigate the effect of phosphorylation and 14–3–3 on vimentin mechanics by studying precise force-strain curves from optical trap experiments. We find that the filaments soften with increasing amount of phosphorylated protein within the filament and that interaction with the protein 14–3–3 further enhances this effect. By combining our me-

chanical measurements with mass spectrometry, cross-linking, phosphomimicri and numeric modeling, we are able to attribute the softening to reduced lateral coupling of monomers within the filaments.

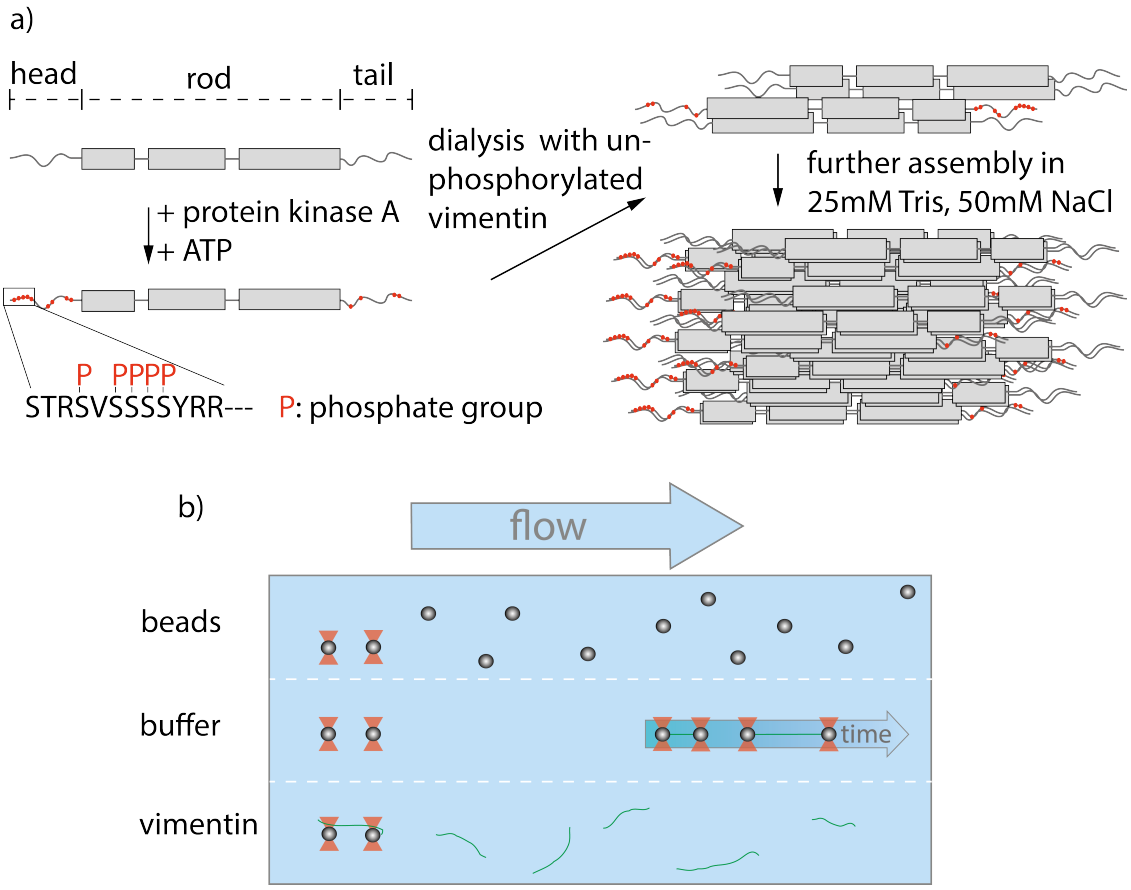

Figure 1: Experimental design and setup. a) Assembly process of partially phosphorylated vimentin. Vimentin monomers consist of a central rod domain flanked by intrinsically disordered head and tail domains. A part of the monomers are phosphorylated by addition of protein-kinase A and ATP leading to several phosphorylated sites in the head and tail, highlighted in red. The phosphorylated monomers are mixed with unphosphorylated vimentin prior to assembly by dialysis into a salt-containing buffer. b) Overview of the microfluidic chip used within the optical trap. The different compartments are realized by laminar flow and the measurements are performed in the buffer region.

To investigate whether phosphorylation of vimentin influences filament mechanics, we record force-strain curves using optical traps. As complete phosphorylation of vimentin filaments leads to disassembly,[21] we perform the stretching experiments on partially phosphorylated vimentin filaments with varying percentages of 1, 5 or 10%, as sketched in Fig. 1a.

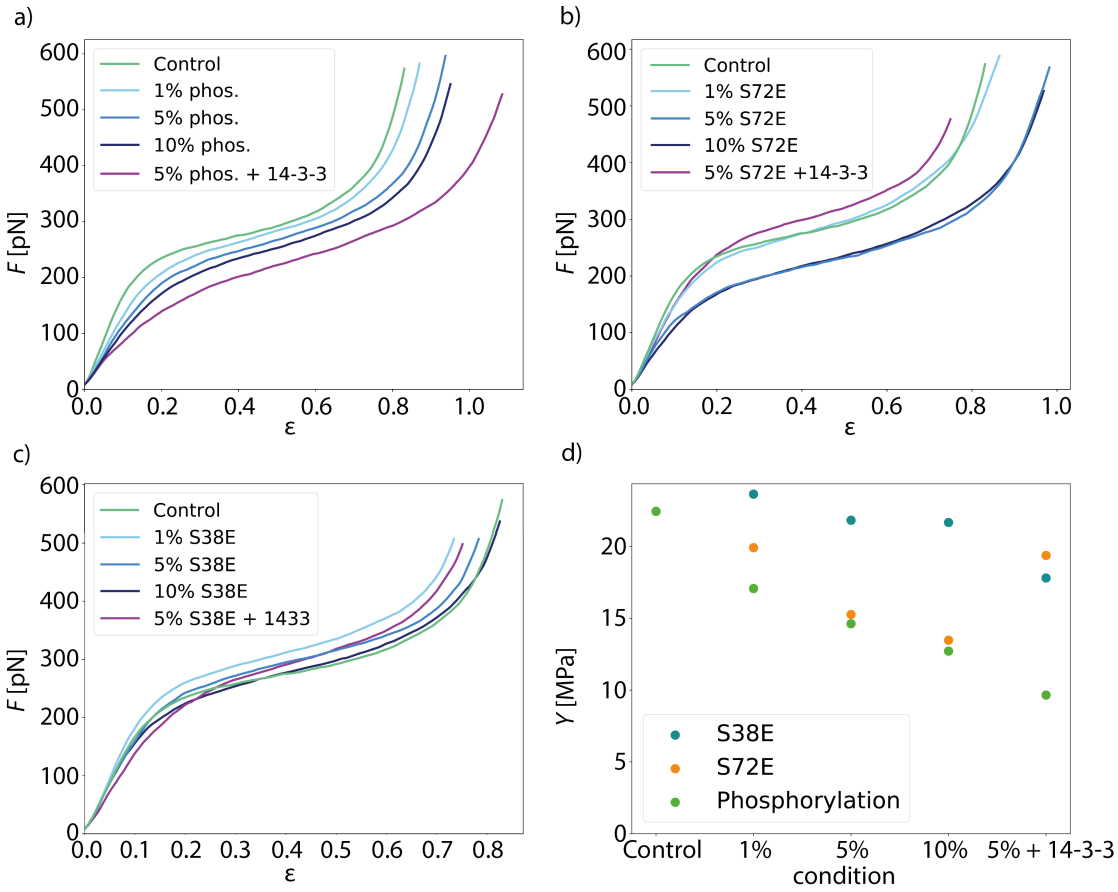

Figure 2: Additional negatively charged amino acids soften vimentin filaments. a) Mean force-strain curves for partially phosphorylated filaments: control (unphosphorylated, green), 1% phosphorylation (light blue), 5% phosphorylation (medium blue), 10% phosphorylation (dark blue) and 5% phosphorylation with 14–3–3 (magenta). With increasing amount of phosphorylated vimentin incorporated, the filaments become softer; the effect is even more pronounced in the presence of the protein 14–3–3. b, c) Mean force-strain curves for the phosphomimicri data. The color code for the individual conditions is the same as in a. b) The mean curves for the phosphomimetic mutant S72E show a similar trend as the phosphorylation data except for the filaments incubated with 14–3–3. c) The mean curves of the phosphomimetic mutant S38E do not show a systematic softening regardless of whether the filaments were incubated with 14–3–3 or not. d) Comparison of the different data sets. The Young's modulus Y, which is a measure of the filament stiffness, is shown in dependence of the amount of phosphorylated or phosphomimetic protein. The phosphoylation (green) and the S72E data (orange) show a softening with increasing phosphorylation or phosphomimicri, whereas the S38E data (blue) remain fairly constant. Incubation with 14–3–3 leads to even softer filaments for phosphoylated vimentin but not for vimentin S72E and S38E filaments.

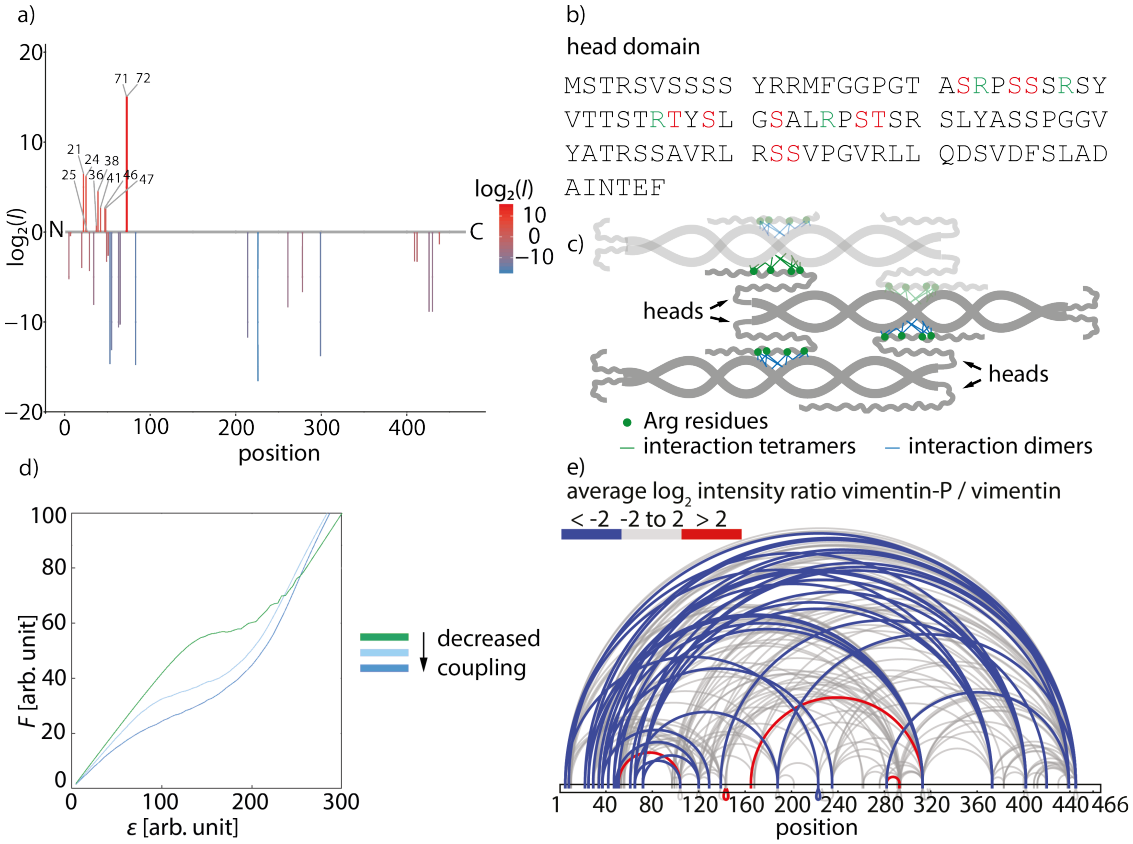

Figure 3: Softening of phosphorylated filaments is due to decreased lateral interactions. a) Determination of phosphorylated sites in vimentin. Phosphorylated peptides are determined by LC-MS and the degree of phosphorylation of all identified sites is plotted using the $\log_2$ ratios of the LC-MS intensities of phosphorylated over non-phosphorylated peptides (intensities I). Identified phosphorylation sites and the numbers of amino acids are listed. The color code represents the degree of phosphorylation of all identified phosphorylation sites. b) The amino acid sequence of the head domain of vimentin with positively charged amino acids (green) and phosphorylation sites (red). c) Sketch of a vimentin tetramer. The positively charged amino acids in the head domains (green dots) interact with the negatively charged coils of the neighbouring dimer. Interactions between dimers are depicted in blue, the neighbouring tetramer is illustrated in light gray and interactions between neighbouring tetramers are shown in green. d) Results of numerical model for the softening of the filaments due to decreased lateral coupling. The influence of decreased coupling is shown in the force-strain plot where the completely coupled system is shown in green and the lateral coupling is decreased from light blue to dark blue. e) Mass spectrometry analysis of cross-linked tetramers. The ratio of the amount of cross-links found in the phosphorylated condition and the unphosphorylated condition is calculated. Linked amino acid positions within a tetramer are indicated by loops and the ratio of cross-links between the phosphorylated and unphosphorylated vimentin tetramers is shown by the color code. Blue loops show a decreased amount of cross-links in the phosphorylated condition, gray loops show no change in the ratio of cross-links between phosphorylated and unphosphorylated condition and red loops show an increase of cross-links in the phosphorylated condition.

The incorporation of the phosphorylated vimentin is confirmed by performing a phosphorylation analysis sodium dodecyl sulfate-polyacrylamide gel electrophoresis (SDS-page), shown in SI Appendix, Fig. S1. The single filaments are covalently bound to two polystyrene beads and each bead is captured in an optical trap for precise force measurements. Additionally, we determine the distance between both beads and calculate the strain as $\varepsilon = \frac{\Delta L}{L_0}$, where L_0 is the original filament length and ΔL the additional extension upon application of a force F. We perform all measurements in the "buffer" channel, *i.e.* without any disturbance from surrounding beads or protein, see Fig. 1b. During stretching, we observe the characteristic response of vimentin to the force, including the linear increase for small strains, the plateau region, where the α helices open up[6,7,14] and the subsequent stiffening of the filaments. We perform all measurements in 5 mM Tris-HCl, 50 mM NaCl, pH 7.5 and the curves are comparable to the ones previously recorded in phosphate buffer.[7,14] Such a typical curve for our standard condition is shown in Fig. 2a, green. We show an average curve here for clarity, however, the individual data sets are shown in the SI Appendix, Fig. S2. The measurements end when the force becomes too large for the optical traps, *i.e.* at roughly 550-600 pN. Fig. 2a also shows corresponding data for filaments containing partially phosphorylated protein (shades of blue, for color code see legend). To quantify the force-strain data, we focus on the Young's modulus, which we calculate from the initial slope in the linear regime up to a force of 130 pN of each curve, as a measure of the filament stiffness. The Young's modulus for the unphosphorylated vimentin filaments is in good agreement with the results found in Ref. 7. The analysis procedure is visualized in SI Appendix, Fig. S3. The Young's moduli plotted in Fig. 2d (green) show a strong decrease with increasing percentage of phosphorylated protein, confirming the impression from Fig. 2a, green to dark blue.

Upon phosphorylation of vimentin by PKA, several amino acids are modified. To determine these sites, we perform an LC-MS (liquid chromatography mass spectrometry) analysis. Fig 3a shows that phosphorylated sites are dispersed throughout the whole protein, but the most abundant ones ($\log_2(I) > 0$) are all found in the head region of vimentin. We employ

phosphomimicri to investigate the effect of certain phosphorylated sites detected here and choose two of the most abundantly phosphorylated sites that also occur *in vivo*, S38 and S72.[21] Using these mutants, we perform the same force-strain measurements as described above for the phosphorylated protein. For the mutant S72E, we observe a similar trend as in the phosphorylation data including enhanced softening, see Fig. 2b, green to dark blue. The individual data sets can be found in the SI Appendix, Fig. S4. On the contrary, Fig. 2c, green to dark blue, shows filaments containing the mutation S38E and no systematic trend is observed. The individual curves are provided in the SI Appendix, Fig. S5. When comparing these three different conditions, *i.e.* phosphorylation, mutation S72E and mutation S38E, we observe that the Young's modulus, and therefore the filament stiffness, decreases with an increasing amount of phosphorylation (green) and mutation S72E (orange) but stays fairly constant for the mutation S38E (blue), see Fig. 2d.

To explain these observations, we consider previous studies that have shown neighboring dimers to be coupled by electrostatic interactions between the positively charged amino acids in the head and the negatively charged coiled-coils[3,27,28] as sketched in Fig. 3c. When vimentin becomes phosphorylated, the positive charges, namely arginine (R) residues, of the head domain are flanked by negative charges of the phosphorylated amino acids as shown in Fig. 3b, which diminishes the electrostatic attraction between the head and the coiled-coils. This observation raises the question of whether the shift in filament stiffness can be explained by weaker coupling. Therefore, we run Monte-Carlo simulations to understand how the coupling of dimers affects the force-strain curves of vimentin by extending the model from Refs. 8,14 as described in detail in the SI Appendix. We model a vimentin monomer by including the α helices in the rod domain as the spring constant κ_α and as elements, which extend in length at a certain force, thereby transitioning to an unfolded state u.[8,14,15] The model in Ref. 8 assumes a strong coupling *within* dimers, tetramers or any other subunit of the ULF and weaker coupling *between* these subunits. In that work, the force-strain curves of filaments with smaller coupled subunits exhibit a lower plateau than the force-strain curves

of filaments with larger coupled subunits. Yet, this model does not explain a pronounced decrease in Young's modulus as observed here.

We supplement the model from Ref. 8 by spring constants κ_{bt}, which represent bonds between tetramers, and κ_{bd} for bonds between dimers within the tetramer. In case of more phosphorylated monomers in the filament, the filament subunits cannot arrange as closely as without phosphorylated monomers because the additional negative charges repel each other. Thus, not all bonds between tetramers and dimers can form, so that the spring constants κ_{bd} and κ_{bt} do not contribute to the overall spring constant and the filaments get softer as shown for the simulated force-strain curves in Fig. 3d. Consequently, the initial slope of the force-strain curves decreases with more phosphorylated monomers as in Fig. 2d.

We confirm these numerical findings with mass spectrometry cross-linking experiments. When comparing cross-linked phosphorylated vimentin tetramers to cross-linked unphosphorylated vimentin tetramers in Fig. 3e, blue lines, fewer cross-links are found in the phosphorylated state. All individual cross-linking positions can be found in the SI Appendix, Fig. S6. This supports our proposal that there are larger distances between neighboring dimers in phosphorylated vimentin which indicates that the lateral coupling of dimers is reduced.

Besides the fact that phosphorylation modifies the protein itself by the addition of a phosphate group, it also creates binding sites for other proteins. For example, phophorylated vimentin is known to bind the protein 14–3–3.[23] This raises the question of whether the binding of the protein 14–3–3 to phosphorylated vimentin also has an effect on the mechanics. To answer this question, optical trap measurements of the vimentin/14–3–3 complex are performed. We confirm the interaction between vimentin and 14–3–3 by performing a streptavidin pulldown assay as shown in the SI Appendix, Fig. S7. Fig. 2a, magenta curve, shows that for phoyphorylated filaments the interaction with 14–3–3 softens the filaments even more. By contrast, the original stiffness of the unphosphorylated filaments is recovered for the mutant S72E, shown by the magenta curve in Fig. 2b, and we observe no influence of 14–3–3 for the mutant S38E, shown by the magenta curve in Fig. 2c. The individual curves

for these experiments are provided in the SI Appendix, Fig. S8. We show, that 14–3–3 binds to the phosphorylated sites in the head domain of vimentin, as confirmed by cross-linking the complex and analyzing it with mass spectrometry, see the SI Appendix, Fig. S9. Assumedly, because of this interaction and the similar size of 14–3–3 compared to vimentin, it forces vimentin subunits further apart and thus enhances the decoupling and softening of vimentin filaments. Mostly, vimentin is cross-linked to position 78 of the amino acid sequence of 14–3–3 as shown in SI Appendix, Fig. S9. By contrast, we cannot unambiguously determine the crosslininking position in the amino acid sequence of vimentin. However, our data show that the amino acids S38 and S72 in vimentin are not the binding sites for 14–3–3 as the complex of the two proteins is retrieved after phosphorylation of the phosphomimetic mutants as confirmed by cross-linking the complex, see SI Appendix, Fig. S10. Additionally, we find that there is no interaction between 14–3–3 and the phosphomimetic mutants S38E and S72E and no complex is formed as confirmed by cross-linking the samples. The corresponding SDS gel is shown in SI Appendix, Fig. S10. Taking these results together, we propose that 14–3–3 protects the protein from phosphatases by binding to strategic phosphorylated sites as suggested in Ref. 29. Due to its large size, it sterically hinders the phosphatases from binding to neighboring amino acid positions. Thereby it keeps the filaments in the soft state for extended times, which might be important for *in vivo* situations.

Previous studies have shown that increased vimentin phosphorylation is required for efficient cellular migration[30] and that it is relevant in metastasis[31,32] which may be linked to a softer vimentin network and therefore render the cells more deformable. In general, phosphorylation controls the assembly and disassembly dynamics of vimentin[21] and in particular the phosphorylation of vimentin leads to disassembly. Phosphatase activity enables recovery to assembled filaments. If 14–3–3 binds to phosphorylated vimentin and inhibits the phosphatase activity, vimentin remains in the phosphorylated state. Such an effect would slow down the assembly dynamics, which is, however, crucial for cell adhesion, migration and signaling.[33] In addition, the vimentin/14–3–3 complex builds a larger ensemble with

the phosphorylated protein beclin1, which then promotes tumorigenesis.[34] It was already suggested that vimentin might be a key regulator of tumorigenic pathways as this complex, namely 14–3–3, vimentin and beclin1, might prevent the dephosphorylation of the proteins within the ensemble and thereby inhibit antitumor activity in cells.[35]

To conclude, we have found a possibility for the missing link between the role of phosphorylation in cancer metastasis and the pronounced motility of metastasizing cells as we directly show how post-translational modifications, *i.e.* phosphorylation, change the mechanical properties of vimentin filaments. Vimentin filaments become softer with increasing amount of phosphorylated vimentin within the filament. The interaction of phosphorylated vimentin with 14–3–3 enhances this effect and may even protect this softer state. We suggest that these changes are induced by less electrostatic coupling within the unit-length filament due to additional negative charges introduced by the phosphate groups and support this assumption by a physical model. We thus hypothesize that cells are able to fine-tune and adapt their mechanical properties locally and within seconds by modifications like phosphorylation according to specific external requirements.

Material and Methods

An extended version of the Materials and Methods section can be found in the SI Appendix.

Vimentin purification

Purification of recombinant human vimentin C328A with additional amino acids GGC at the C-terminus based on Herrmann *et al.*[28] was performed according to the protocol described in Ref. 14. The additional amino acids were included to enable binding of the vimentin filaments to maleimide-functionalized beads. Two phosphomimetic mutants of this vimentin C328A, S38E and S72E, were produced according to the same protocol.

14–3–3 purification

Recombinant maltose-binding protein (MBP)-tagged protein 14–3–3γ was expressed and purified from *E. coli* strain BL21 Rosetta. For the actual measurements the MBP-tag was removed from 14–3–3.

Vimentin filament preparation and bead functionalization

Vimentin was fluorescently labeled with ATTO647N *via* maleimide chemistry according to the protocol published in Ref. 7 to enable visualization of the filaments during the optical trapping experiments. To prepare the protein for filament assembly, the protein in storage buffer (8 M Urea, 5 mM Tris-HCl, 1 mM EDTA, 0.1 mM EGTA, 0.01 mM MAC and 250 mM KCl, pH 7.5) was dialyzed into 6 M Urea, 5 mM Tris-HCl at pH 8.4 and a stepwise dialysis to 5 mM Tris-HCl, pH 8.4 was performed. To initiate the assembly, the protein was dialyzed into 25 mM Tris-HCl, pH 7.5 with 50 mM NaCl over night. The final amount of labeled monomers within the filaments was about 4%. In analogy to the assembly of phosphorylated vimentin, the phosphomimetic mutants were mixed with vimentin C328A at mixing ratios of 1%, 5% and 10%. The mixing was performed in 8 M urea, *i.e.* prior to the dialysis step to ensure mixing at the monomer state of vimentin.

The beads were functionalized with maleimide according to Ref. 36.

Phosphorylation of vimentin

We phosphorylated vimentin tetramers in 5 mM Tris-HCl, pH 8.4 using cAMP-dependent protein kinase A (New England Biolabs, Frankfurt, Germany). The phosphorylated vimentin was mixed at the desired ratios of 1, 5 and 10% with unphosphorylated vimentin. Subsequently, a stepwise dialysis and the assembly were performed as described above.

Degree of phosphorylation in tetramers and filaments

To test whether the phosphorylation of vimentin tetramers was successful, phosphorylation analysis gels (Phos-tag Acrylamide AAL-107, FUJIFILM Wako Chemicals Europe GmbH, Neuss, Germany) were used. These gels show additional bands above the actual protein band if the protein is phosphorylated successfully.

Verification of vimentin binding to 14–3–3

To test whether the binding of 14–3–3 to vimentin was successful, a streptavidin pulldown assay was performed (adapted from Ref. 37).

Binding 14–3–3 to vimentin filaments

To bind the protein 14–3–3 to vimentin it was first diluted to the same concentration determined in g/L as the vimentin solution. Then, 14–3–3 and assembled vimentin filaments were mixed at a ratio of 1:1 with respect to the concentration in g/L and incubated for 1 h at 37°C. For the optical trap measurements, 30 μL of this solution were diluted by 1 mL assembly buffer (25 mM Tris-HCl, pH 7.5 and 50 mM NaCl).

Optical trap measurements and analysis

For all measurements a commercial optical trap setup (C-trap, Lumicks, Netherlands) was used, which combines the optical traps with a microfluidic chip and confocal microscopy. For each measurement a fresh pair of beads was captured in the bead channel (see Fig.1b). The beads were moved to the buffer channel (containing pure assembly buffer) for calibration. Afterwards they were moved to the vimentin channel (containing vimentin filaments in assembly buffer), while scanning with the confocal microscope, until a single vimentin filament was captured on one bead. Then, the beads were moved back to the buffer channel where the filament was attached to the second bead. We ensured that the filament was relaxed

to avoid prestrain. The measurements were performed by moving one bead with a constant speed of about 0.7 μm/s to stretch the filament until it ruptured or the forces on the second bead were higher than the power of the trap. During the stretching, force-distance curves were recorded.

All data were saved as hdf5-files and then further analyzed with self-written Python codes. To obtain the force-strain curves for each measurement, the strain was calculated by $\varepsilon = \frac{\Delta L}{L_0}$, with the initial length of the filament L_0 (defined at a force of 5 pN) and the difference in length between stretched and the initial state ΔL. The calculation of the mean curves for each conditions was adapted from Ref. 8. For the calculation of the Young's modulus, a linear fit up to a force of 130 pN was performed for the initial slope in the linear regime of the mean force-strain curves. The Young's modulus was calculated *via* the ratio of stress and strain, $Y = \frac{\sigma}{\varepsilon} = \frac{F/\pi r^2}{\varepsilon}$. The radius r was set constant to 5 nm.

Cross-linking experiments with mass spectrometry

Phosphorylated and non-phosphorylated vimentin was cross-linked in presence of 14–3–3 protein to determine the interaction sites of the two proteins after phosphorylation. For the main experiment, samples were cross-linked with a 500 and 1,000 fold molar excess of bis(sulfosuccinimidyl)suberate (BS^3; Thermo Fisher Scientific, Kandel, Germany) and the corresponding bands were cut, in-gel digested, and peptides were extracted as described elsewhere.[38]

A quantitative cross-linking approach was pursued to examine the structural changes of vimentin caused by phosphorylation. To do so, phosphorylated, and non-phosphorylated vimentin samples were cross-linked with differentially isotope-labelled disuccinimidyl suberate (DSS; Thermo Fisher Scientific) containing either zero or four deuterium atoms. Then phosphorylated and non-phosphorylated vimentin samples cross-linked with the opposite isotopic labels were mixed in equal ratios and the labels were swapped for a second reaction replicate.

Data analysis of mass spectrometry experiments

Raw files were submitted to a cross-link database search with pLink 2 (version 2.3.9)[39] against the sequences of human vimentin and 14–3–3. Database searches of quantitative cross-linking acquisitions were performed with pLink 1 (version 1.23),[40] because of the possibility to specify narrow mass windows and thereby exclude the isotope signals derived from the heavy cross-linker. Quantification was performed with XiQ.[41] Cross-links were visualized on proteins with xiNET[42] and quantitative values were plotted with Perseus.[43]

Analysis of phosphorylated and non-phosphorylated peptides was performed in MaxQuant version 1.6.2.10[44,45] using reviewed human protein sequences from Uniprot (02/2019)[46] supplemented with the modified vimentin sequence. Phosphorylation of serine, threonine, and tyrosine was added to variable modifications. Other settings were kept default. Peptide peak intensities were extracted using Skyline version 19.1.0.193.[47] Intensities of phosphorylated peptides were normalized by intensities of the corresponding non-phosphorylated peptides using a custom R script.

Model

To simulate the force-strain behavior of a vimentin IF, we calculated all spring constants of the modeled elements and transition rates of possible reactions and ran a Monte-Carlo simulation with a self-written Matlab code (MathWorks, Natick, Massachusetts, USA) as in Ref. 8,14.

Acknowledgement

The authors thank Susanne Bauch for preparing the vimentin protein, Monika Raabe for carrying out the phosphopeptide enrichment and Harald Herrmann for helpful discussions. This work was financially supported by the European Research Council (ERC) under the European Unions Horizon 2020 research and innovation program (Consolidator Grant Agreement

no. 724932, to S.K.). Further financial support was received from the Deutsche Forschungsgemeinschaft (DFG) in the framework of SFB 860 (project number B10, to S.K.), SFB 1286 (project number A08, to H.U.) and the Cluster of Excellence "Multiscale Bioimaging: from Molecular Machines to Networks of Excitable Cells" (MBExC, to S.K. and B.S.). C.L. received a fellowship of the Studienstiftung des deutschen Volkes.

Author Contributions

S.K. conceived and supervised the project. J.K. performed the experiments and analyzed the data. J.M. and B.S. provided the 14–3–3 protein. H.U., I. P. and I. S. performed the mass spectrometry measurements. C.L. performed the numerical simulations. J.K. and S.K. wrote the manuscript with contributions from all authors.

Competing interests

The authors declare no competing interests.

Data availability

The data that support the findings of this study are available from the corresponding authors upon reasonable request.

References

(1) Huber, F.; Boire, A.; Preciado López, M.; Koenderink, G. H. Cytoskeletal crosstalk: when three different personalities team up. *Current Opinion in Cell Biology* **2015**, *32*, 39–47.

(2) Szeverenyi, I.; Cassidy, A. J.; Chung, C. W.; Lee, B. T.; Common, J. E. The human intermediate filament database: Comprehensive information on a gene family involved in many human diseases. *Human Mutation* **2008**, *29*, 351–360.

(3) Herrmann, H.; Häner, M.; Brettel, M.; Müller, S. A.; Goldie, K. N.; Fedtke, B.; Lustig, A.; Franke, W. W.; Aebi, U. Structure and Assembly Properties of the Intermediate Filament Protein Vimentin: The Role of its Head, Rod and Tail Domains. *J. Mol. Biol.* **1996**, *264*, 933–953.

(4) Chernyatina, A. A.; Guzenko, D.; Strelkov, S. V. Intermediate filament structure: the bottom-up approach. *Current Opinion in Cell Biology* **2015**, *32*, 65 – 72, Cell architecture.

(5) Herrmann, H.; Aebi, U. Intermediate Filaments: Strucutre and Assembly. *Cold Spring Harb. Perspect. Biol.* **2016**, *8*, a018242.

(6) Qin, Z.; Kreplak, L.; Buehler, M. Hierarchical structure controls nanomechanical properties of vimentin intermediate filaments. *PLoS ONE* **2009**, *4*, 1–14.

(7) Block, J.; Witt, H.; Candelli, A.; Peterman, E. J. G.; Wuite, G. J. L.; Janshoff, A.; Köster, S. Nonlinear Loading-Rate-Dependent Force Response of Individual Vimentin Intermediate Filaments to Applied Strain. *Physical Review Letters* **2017**, *118*, 1–5.

(8) Lorenz, C.; Forsting, J.; Schepers, A. V.; Kraxner, J.; Bauch, S.; Witt, H.; Klumpp, S.; Köster, S. Lateral Subunit Coupling Determines Intermediate Filament Mechanics. *Phys. Rev. Lett.* **2019**, *123*, 188102.

(9) Eriksson, J. E.; Dechat, T.; Grin, B.; Helfand, B.; Mendez, M.; Palari, H.-M.; Goldman, R. D. Introducing intermediate filaments: from discovery to disease. *J. Clin. Invest.* **2009**, *119*, 1763–1771.

(10) Kreplak, L.; Bär, H.; Leterrier, J. F.; Herrmann, H.; Aebi, U. Exploring the mechanical behavior of single intermediate filaments. *Journal of Molecular Biology* **2005**, *354*, 569–577.

(11) Kreplak, L.; Herrmann, H.; Aebi, U. Tensile Properties of Single Desmin Intermediate Filaments. *Biophysical Journal* **2008**, *94*, 2790 – 2799.

(12) Ackbarow, T.; Buehler, M. Superelasticity, energy dissipation and strain hardening of vimentin coiled-coil intermediate filaments: atomistic and continuum studies. *Journal of Materials Science* **2007**, *42*, 8771–8787.

(13) Pinto, N.; Yang, F.-C.; Negishi, A.; Rheinstädter, M. C.; Gillis, T. E.; Fudge, D. S. Self-Assembly Enhances the Strength of Fibers Made from Vimentin Intermediate Filament Proteins. *Biomacromolecules* **2014**, *15*, 574–581.

(14) Block, J.; Witt, H.; Candelli, A.; Danes, J. C.; Peterman, E. J.; Wuite, G. J.; Janshoff, A.; Köster, S. Viscoelastic properties of vimentin originate from nonequilibrium conformational changes. *Science Advances* **2018**, *4*.

(15) Forsting, J.; Kraxner, J.; Witt, H.; Janshoff, A.; Köster, S. Vimentin Intermediate Filaments Undergo Irreversible Conformational Changes during Cyclic Loading. *Nano Letters* **2019**, *19*, 7349–7356.

(16) Fuchs, E.; Cleveland, D. W. A Structural Scaffolding of Intermediate Filaments in Health and Disease. *Science* **1998**, *279*, 514–519.

(17) Schepers, A. V.; Lorenz, C.; Köster, S. Tuning Intermediate Filament Mechanics by Variation of pH and Ion Charges. *bioRxiv* **2020**,

(18) Hyder, C. L.; Pallari, H.-M.; Kochin, V.; Eriksson, J. E. Providing cellular signposts - Post-translational modifications of intermediate filaments. *FEBS Letters* **2008**, *582*, 2140–2148.

(19) Snider, N. T.; Omary, M. B. Post-translational modifications of intermediate filament proteins: mechanisms and functions. *Nature Reviews Molecular Cell Biology* **2014**, *15*, 163–177.

(20) Busch, T.; Armacki, M.; Eiseler, T.; Joodi, G.; Temme, C.; Jansen, J.; von Wichert, G.; Omary, M. B.; Spatz, J.; Seufferlein, T. Keratin 8 phosphorylation regulates keratin reorganization and migration of epithelial tumor cells. *Journal of Cell Science* **2012**, *125*, 2148–2159.

(21) Eriksson, J. E.; He, T.; Trejo-Skalli, A. V.; Harmala-Brasken, A. S.; Hellman, J.; Chou, Y.-H. H.; Goldman, R. D.; Härmälä-Braskén, A.-S.; Hellman, J.; Chou, Y.-H. H.; Goldman, R. D. Specific in vivo phosphorylation sites determine the assembly dynamics of vimentin intermediate filaments. *Journal of Cell Science* **2004**, *117*, 919–932.

(22) Traub, P.; Vorgias, C. E. Involvement of the N-terminal polypeptide of vimentin in the formation of intermediate filaments. *Journal of Cell Science* **1983**, *63*, 43–67.

(23) Tzivion, G.; Luo, Z. J.; Avruch, J. Calyculin A-induced vimentin phosphorylation sequesters 14-3-3 and displaces other 14-3-3 partners in vivo. *Journal of Biological Chemistry* **2000**, *275*, 29772–29778.

(24) Gardino, A. K.; Yaffe, M. B. 14-3-3 proteins as signaling integration points for cell cycle control and apoptosis. *Seminars in Cell & Developmental Biology* **2011**, *22*, 688 – 695.

(25) Ku, N.-O.; Michie, S.; Resurreccion, E. Z.; Broome, R. L.; Omary, M. B. Keratin binding to 14-3-3 proteins modulates keratin filaments and hepatocyte mitotic progression. *Proc. Natl. Acad. Sci. U.S.A.* **2002**, *99*, 4373–4378.

(26) Miao, L.; Teng, J.; Lin, J.; Liao, X.; Chen, J. 14-3-3 proteins interact with neurofilament protein-L and regulate dynamic assembly of neurofilaments. *Journal of Cell Science* **2013**, *126*, 427–436.

(27) Parry, D. A.; Steinert, P. M. *Intermediate filament structure*; Springer-Verlag, 1995; p 183 pp.

(28) Herrmann, H.; Aebi, U. Intermediate Filaments: Molecular Structure, Assembly Mechanism, and Integration Into Functionally Distinct Intracellular Scaffolds. *Annual Review of Biochemistry* **2004**, *73*, 749–789.

(29) Smith, A. J.; Daut, J.; Schwappach, B. Membrane proteins as 14-3-3 clients in functional regulation and intracellular transport. *Physiology* **2011**, *26*, 181–191.

(30) Barberis, L.; Pasquali, C.; Bertschy-Meier, D.; Cuccurullo, A.; Costa, C.; Ambrogio, C.; Vilbois, F.; Chiarle, R.; Wymann, M.; Altruda, F.; Rommel, C.; Hirsch, E. Leukocyte transmigration is modulated by chemokine-mediated PI3Kγ-dependent phosphorylation of vimentin. *European Journal of Immunology* **2009**, *39*, 1136–1146.

(31) Lim, Y.-P.; Wong, C. Y.; Ooi, L. L.; Druker, B. J.; Epstein, R. J. Selective Tyrosine Hyperphosphorylation of Cytoskeletal and Stress Proteins in Primary Human Breast Cancers. *Clinical Cancer Research* **2004**, *10*, 3980–3987.

(32) Zhu, Q. et al. Vimentin is a novel AKT1 target mediating motility and invasion. *Oncogene* **2011**, *30*, 457–470.

(33) Ivaska, J.; Pallari, H.-M.; Nevo, J.; Eriksson, J. E. Novel functions of vimentin in cell adhesion, migration, and signaling. *Experimental Cell Research* **2007**, *313*, 2050 – 2062, Special Issue - Intermediate Filaments.

(34) Wang, R. C.; Wei, Y.; An, Z.; Zou, Z.; Xiao, G.; Bhagat, G.; White, M.; Reichelt, J.; Levine, B. Akt-Mediated Regulation of Autophagy and Tumorigenesis Through Beclin 1 Phosphorylation. *Science* **2012**, *338*, 956–959.

(35) Kidd, M. E.; Shumaker, D. K.; Ridge, K. M. The Role of Vimentin Intermediate Fil-

aments in the Progression of Lung Cancer. *American Journal of Respiratory Cell and Molecular Biology* **2014**, *50*, 1–6.

(36) Janissen, R.; Berghuis, B. A.; Dulin, D.; Wink, M.; Van Laar, T.; Dekker, N. H. Invincible DNA tethers: Covalent DNA anchoring for enhanced temporal and force stability in magnetic tweezers experiments. *Nucleic Acids Research* **2014**, *42*, e137.

(37) Kilisch, M.; Lytovchenko, O.; Arakel, E. C.; Bertinetti, D.; Schwappach, B. A dual phosphorylation switch controls 14-3-3-dependent cell surface expression of TASK-1. *Journal of Cell Science* **2016**, *129*, 831–842.

(38) Schmidt, C.; Urlaub, H. iTRAQ-Labeling of In-Gel Digested Proteins for Relative Quantification. *Methods in Molecular Biology (Clifton, N.J.)* **2009**, *564*, 207–226.

(39) Chen, Z. L. et al. A high-speed search engine pLink 2 with systematic evaluation for proteome-scale identification of cross-linked peptides. *Nat. Communications* **2019**, *10*.

(40) Yang, B. et al. Identification of cross-linked peptides from complex samples. *Nat. Methods* **2012**, *9*, 904—906.

(41) Fischer, L.; Chen, Z. A.; Rappsilber, J. Quantitative cross-linking/mass spectrometry using isotope-labelled cross-linkers. *Journal of Proteomics* **2013**, *88*, 120–128.

(42) Combe, C. W.; Fischer, L.; Rappsilber, J. xiNET: cross-link network maps with residue resolution. *Molecular & Cellular Proteomics* **2015**, *14*, 1137–1147.

(43) Tyanova, S.; Temu, T.; Sinitcyn, P.; Carlson, A.; Hein, M. Y.; Geiger, T.; Mann, M.; Cox, J. The Perseus computational platform for comprehensive analysis of (prote) omics data. *Nat. Methods* **2016**, *13*, 731.

(44) Cox, J.; Mann, M. MaxQuant enables high peptide identification rates, individualized ppb-range mass accuracies and proteome-wide protein quantification. *Nature Biotechnology* **2008**, *26*, 1367–1372.

(45) Tyanova, S.; Temu, T.; Cox, J. The MaxQuant computational platform for mass spectrometry-based shotgun proteomics. *Nature Protocols* **2016**, *11*, 2301.

(46) Consortium, U. UniProt: a worldwide hub of protein knowledge. *Nucleic Acids Research* **2019**, *47*, D506–D515.

(47) MacLean, B.; Tomazela, D. M.; Shulman, N.; Chambers, M.; Finney, G. L.; Frewen, B.; Kern, R.; Tabb, D. L.; Liebler, D. C.; MacCoss, M. J. Skyline: an open source document editor for creating and analyzing targeted proteomics experiments. *Bioinformatics* **2010**, *26*, 966–968.